NASA/TM-20210009690

Thermal Expansion Coefficients of $Ca_2Y_8(SiO_4)_6O_2$ and $Ca_2Yb_8(SiO_4)_6O_2$ Apatite-Type Silicates

Jamesa L. Stokes
Glenn Research Center, Cleveland, Ohio

April 2021

NASA STI Program . . . in Profile

Since its founding, NASA has been dedicated to the advancement of aeronautics and space science. The NASA Scientific and Technical Information (STI) Program plays a key part in helping NASA maintain this important role.

The NASA STI Program operates under the auspices of the Agency Chief Information Officer. It collects, organizes, provides for archiving, and disseminates NASA's STI. The NASA STI Program provides access to the NASA Technical Report Server—Registered (NTRS Reg) and NASA Technical Report Server—Public (NTRS) thus providing one of the largest collections of aeronautical and space science STI in the world. Results are published in both non-NASA channels and by NASA in the NASA STI Report Series, which includes the following report types:

- TECHNICAL PUBLICATION. Reports of completed research or a major significant phase of research that present the results of NASA programs and include extensive data or theoretical analysis. Includes compilations of significant scientific and technical data and information deemed to be of continuing reference value. NASA counter-part of peer-reviewed formal professional papers, but has less stringent limitations on manuscript length and extent of graphic presentations.

- TECHNICAL MEMORANDUM. Scientific and technical findings that are preliminary or of specialized interest, e.g., "quick-release" reports, working papers, and bibliographies that contain minimal annotation. Does not contain extensive analysis.

- CONTRACTOR REPORT. Scientific and technical findings by NASA-sponsored contractors and grantees.

- CONFERENCE PUBLICATION. Collected papers from scientific and technical conferences, symposia, seminars, or other meetings sponsored or co-sponsored by NASA.

- SPECIAL PUBLICATION. Scientific, technical, or historical information from NASA programs, projects, and missions, often concerned with subjects having substantial public interest.

- TECHNICAL TRANSLATION. English-language translations of foreign scientific and technical material pertinent to NASA's mission.

For more information about the NASA STI program, see the following:

- Access the NASA STI program home page at http://www.sti.nasa.gov

- E-mail your question to help@sti.nasa.gov

- Fax your question to the NASA STI Information Desk at 757-864-6500

- Telephone the NASA STI Information Desk at 757-864-9658

- Write to:
  NASA STI Program
  Mail Stop 148
  NASA Langley Research Center
  Hampton, VA 23681-2199

NASA/TM-20210009690

Thermal Expansion Coefficients of $Ca_2Y_8(SiO_4)_6O_2$ and $Ca_2Yb_8(SiO_4)_6O_2$ Apatite-Type Silicates

Jamesa L. Stokes
Glenn Research Center, Cleveland, Ohio

National Aeronautics and
Space Administration

Glenn Research Center
Cleveland, Ohio 44135

April 2021

Acknowledgments

The author thanks Bryan Harder for helpful discussions and technical review.

This report contains preliminary findings, subject to revision as analysis proceeds.

Level of Review: This material has been technically reviewed by technical management.

Available from

NASA STI Program
Mail Stop 148
NASA Langley Research Center
Hampton, VA 23681-2199

National Technical Information Service
5285 Port Royal Road
Springfield, VA 22161
703-605-6000

This report is available in electronic form at http://www.sti.nasa.gov/ and http://ntrs.nasa.gov/

Thermal Expansion Coefficients of $Ca_2Y_8(SiO_4)_6O_2$ and $Ca_2Yb_8(SiO_4)_6O_2$ Apatite-Type Silicates

Jamesa L. Stokes
National Aeronautics and Space Administration
Glenn Research Center
Cleveland, Ohio 44135

Summary

High-temperature x-ray diffraction scans of $Y_2Si_2O_7$ and $Yb_2Si_2O_7$ reactions with calcium-magnesium-aluminosilicates were utilized to determine thermal expansion coefficients (CTEs) of $Ca_2Y_8(SiO_4)_6O_2$ and $Ca_2Yb_8(SiO_4)_6O_2$ apatite materials. In order to validate these measurements, the CTEs of $Y_2Si_2O_7$ and $Yb_2Si_2O_7$ were also determined from the same scans. The directional CTEs for γ-$Y_2Si_2O_7$ were determined to be $\alpha_a = 5.84\times10^{-6}$/K, $\alpha_b = 6.81\times10^{-6}$/K and $\alpha_c = 0.81\times10^{-6}$/K, and β-$Yb_2Si_2O_7$ was determined to have values of $\alpha_a = 6.89\times10^{-6}$/K, $\alpha_b = 4.81\times10^{-6}$/K and $\alpha_c = 2.78\times10^{-6}$/K. The average CTEs of γ-$Y_2Si_2O_7$ and β-$Yb_2Si_2O_7$ were determined to be 4.49×10^{-6}/K and 4.82×10^{-6}/K, respectively, which agreed with previous analyses. $Ca_2Y_8(SiO_4)_6O_2$ exhibited directional CTEs of $\alpha_a = 9.36\times10^{-6}$/K and $\alpha_c = 7.95\times10^{-6}$/K (averaged between two sets of data), whereas $Ca_2Yb_8(SiO_4)_6O_2$ had values that were very similar ($\alpha_a = 9.63\times10^{-6}$/K and $\alpha_c = 7.45\times10^{-6}$/K). Both results for the rare-earth (RE) $Ca_2RE_8(SiO_4)_6O_2$ apatites correlated well with the limited data on apatite-type silicates available in literature.

1.0 Introduction

Silicon carbide- (SiC-) based ceramic matrix composites (CMCs) are being incorporated into gas turbine engines to replace traditional metallic components due to their lower densities and higher temperature stability. Due to the reactions with water vapor in the combustion environment, these materials require a protective coating for the long life required for turbine engine applications (Refs. 1 and 2). Environmental barrier coatings (EBCs) are an enabling technology for CMCs, as they protect these materials from water-vapor-induced oxidation and volatilization. Rare-earth (RE) silicates like yttrium disilicate ($Y_2Si_2O_7$) and ytterbium disilicate ($Yb_2Si_2O_7$) are considered state-of-the-art EBC materials because they exhibit thermal expansion coefficients (CTEs) close to SiC-based ceramics (~4 to 5×10^{-6}/K) (Ref. 3) and possess good stability at high temperatures. However, there are several degradation mechanisms that can lead to damage and spallation of the coatings (Ref. 4).

1.1 Thermochemical Degradation of EBCs

With continuous emphasis on increasing operating temperature of gas turbine engine systems to improve efficiency, a concern has arisen in regards to thermochemical interactions of coating materials with dust particulates ingested into the engine during operation. At lower temperatures, interactions with these particulates are largely mechanical, resulting in coating erosion (Ref. 5). At higher temperatures, these dust particulates, primarily made up of calcium-magnesium-aluminosilicates (CMASs), can react with coatings and form amorphous and crystalline phases based on the thermodynamic equilibria with the starting coating material. The resulting phases often have thermal and mechanical properties vastly different from the EBC material (Refs. 6 and 7). Therefore, it is desirable to characterize the behavior of these phases at high temperature.

1.2 Yttrium and Ytterbium Disilicate Interactions With Calcium-Magnesium-Aluminosilicates

CMAS interactions with yttrium (YDS) and ytterbium disilicate (YbDS) have been previously investigated using furnace heat treatments and in situ high-temperature x-ray diffraction (XRD) scans of mixed disilicate and CMAS powders (Ref. 8). More details can be found in the published investigation, but the relevant results are summarized as follows: in this study, three CMAS powders were synthesized based on varying $CaO:SiO_2$ ratios of dust particulates from relevant operating environments, including desert sand and volcanic ash. The CMAS compositions are referred to as CMAS–1 (30.67CaO-8.25MgO-12.81$AlO_{1.5}$-48.27SiO_2), CMAS–2 (24.82CaO-9.08MgO-14.24$AlO_{1.5}$-51.86SiO_2), and CMAS–3 (6.74CaO-8.89MgO-14.23$AlO_{1.5}$-70.14SiO_2). These CMAS powders were then mixed with YDS and YbDS in a 50:50 mol% ratio. Exposure of the disilicate mixtures to temperatures above the CMAS melting temperature resulted in dissolution into the molten glass. Reaction products included reprecipitation of the disilicate phase and a $Ca_2RE_8(SiO_4)_6O_2$ apatite-type silicate, which is an isomorph of the calcium hydroxyapatite mineral $Ca_{10}(PO_4)_6(OH)_2$. In Stokes et al. (Ref. 8), apatite formation was observed to decrease linearly with $CaO:SiO_2$ ratio, likely due to the reduced stability of smaller RE cations like Yb^{3+} or Y^{3+} in the apatite structure, as CaO is a main stabilizer of the Ca-RE apatite phase (Ref. 9).

This apatite-type silicate has been considered a beneficial phase in CMAS mitigation. Within thermal barrier coating (TBC) systems based on RE zirconates ($RE_2Zr_2O_7$), the apatite phase was shown to crystallize rapidly when coatings reacted with molten CMAS, forming a barrier layer at the surface to prevent further infiltration and interaction of the melt (Ref. 10). Based on such studies, several investigations have focused on promoting apatite formation in coating systems or using apatite materials as coatings. As previously stated, an important consideration for prospective EBC materials is a good CTE match with the SiC substrate to minimize mismatch strains. Unfortunately, there is a dearth of knowledge in literature for the calcium RE apatites CTEs. Therefore, the goal of this report is to investigate the thermal expansion behavior of the apatite-type materials resulting from the thermochemical interactions with CMAS.

1.3 High-Temperature X-Ray Diffraction

New data was not acquired for this report, but instead, as mentioned in the previous section, in situ XRD scans of reactions YDS and YbDS with the aforementioned CMAS compositions at temperature were previously obtained in Reference 8. These reactions resulted in the formation of the Ca-RE apatite-type silicates $Ca_2Y_8(SiO_4)_6O_2$ and $Ca_2Yb_8(SiO_4)_6O_2$, respectively. Figure 1 displays the in situ XRD scans obtained for the mixtures of CMAS–1 with YDS (Figure 1(a)) and YbDS (Figure 1(b)) from that study (YDS:CMAS–1 and YbDS:CMAS–1). Scans of CMAS interactions were taken at 25, 500, 900, 1,100, and 1,200 °C. Then the samples were held at 1,200 °C and scans were taken every 2 min at temperature to observe the evolution of crystallization products as a function of time. Finally, a scan was taken at 1,400 °C, then again at 25 °C upon cooling.

In the case of YDS:CMAS–1 (as shown in Figure 1(a)), the apatite phase was not detected in the XRD scans until 1,100 °C, at which the apatite phase was observable in very small amounts. At 1,200 °C, however, more apatite crystallized and constituted more than half of the sample, with additional apatite crystallizing until the starting YDS was not detectable around ~20 min into the exposure at temperature. Heating to 1,400 °C did not result in an observable change in apatite content, and the final scan at 25 °C indicated that reactions of YDS with CMAS–1 resulted in the full conversion of YDS to apatite. It was shown in the previous publication that YDS reacted with CMAS–2 to form apatite, with apatite peaks also

being observed starting at 1,100 °C. Because of the lower CaO content of CMAS–2 compared to CMAS–1, however, the full conversion of YDS to apatite did not occur and the YDS phase was present in the sample in all scans. Thus, for $Ca_2Y_8(SiO_4)_6O_2$, data was obtained in both YDS:CMAS–1 and YDS:CMAS–2 at 25 °C upon cooling, as well as 1,200 and 1,400 °C. Conversely, very little apatite formed in YbDS:CMAS–1 below 1,400 °C. This was determined to be due to the thermodynamic equilibria resulting in phases like grossular garnet and a Ca-Yb cyclosilicate instead of apatite at lower temperatures (Figure 1(b)). Therefore, data for $Ca_2Yb_8(SiO_4)_6O_2$ was only obtained at 25 °C upon cooling and at 1,400 °C. Although apatite formed at 1,400 °C and was observed at 25 °C upon cooling, the starting YbDS phase remained present in all YbDS:CMAS–1 scans. $Ca_2Yb_8(SiO_4)_6O_2$ did not crystallize in YbDS interactions with CMAS–2 or CMAS–3 due to the smaller RE cation size as well as reduced CaO content in the CMAS compositions.

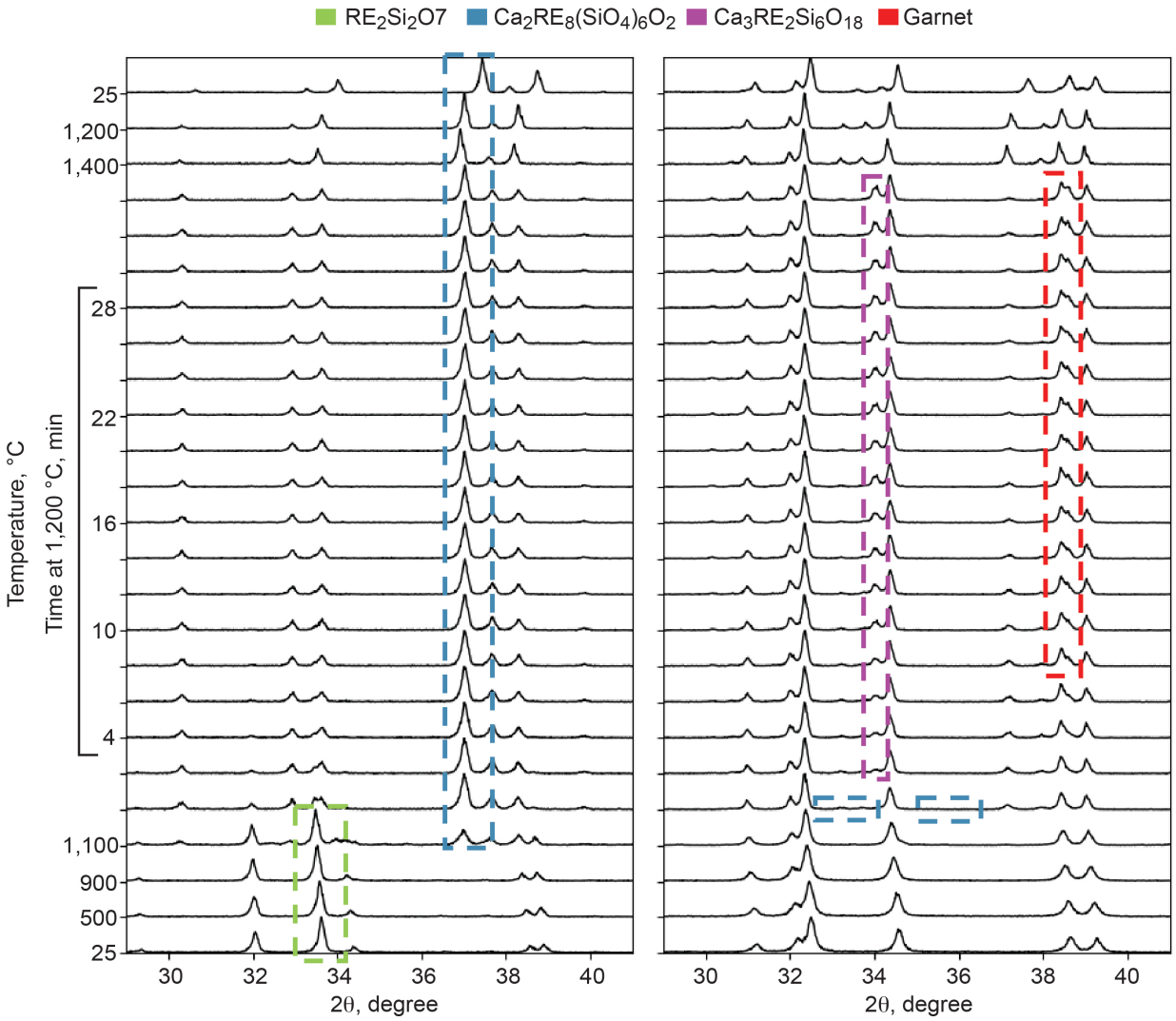

Figure 1.—In situ x-ray diffraction scans up to 1,400 °C of yttrium (YDS) and ytterbium (YbDS) disilicate with calcium-magnesium-aluminosilicate (CMAS). CMAS–1 is $30.67CaO\text{-}8.25MgO\text{-}12.81AlO_{1.5}\text{-}48.27SiO_2$. Angle at which each data point was taken on the graph (θ). (a) YDS:CMAS–1. (b) YbDS:CMAS–1. The highest intensity peaks of the calcium rare-earth (Ca-RE) apatite and disilicate phases are identified with the blue and green dashed rectangles, respectively. The cyclosilicate peak is highlighted by the pink dashed rectangle. The shoulder of the YbDS peak around 38.5° is attributed to the garnet phase (red highlighted area).

The aforementioned scans from these high-temperature reaction experiments were utilized in this study to calculate CTEs of apatite structures by determining the change in lattice parameters of the crystalline phases present in the reactions as a function of temperature. As noted, because YDS and YbDS are also present in these scans, the CTEs of these two EBC materials were calculated as well. The thermal expansion behavior of both materials has been characterized in literature, so the calculations of YDS and YbDS CTEs in this report were compared to known values to provide validation of the CTEs calculated in this report for $Ca_2Y_8(SiO_4)_6O_2$ and $Ca_2Yb_8(SiO_4)_6O_2$.

Lattice parameters of YDS, YbDS, $Ca_2Y_8(SiO_4)_6O_2$, and $Ca_2Yb_8(SiO_4)_6O_2$ were derived from the XRD scans at each temperature using the DIFFRAC.TOPAS software package (Bruker) (Ref. 11). The change in lattice parameter ($\Delta L/L_0$) was calculated for each lattice direction and the CTE for each direction was determined as the slope of a linear fit of $\Delta L/L_0$ with temperature in Kelvin from 25 to 1,400 °C.

2.0 Results

2.1 β-$Yb_2Si_2O_7$ and γ-$Y_2Si_2O_7$

YDS exhibited the γ-$RE_2Si_2O_7$ polymorph of the RE disilicates, which is in the monoclinic space group $P2_1/c$, and no phase change of YDS was observed in this study. YDS can exhibit at least four different polymorphs as a function of temperature, although γ-$Y_2Si_2O_7$ exhibits stability over the greatest temperature range and is the polymorph of interest in this work (Ref. 12). The obtained lattice parameters for γ-YDS in interactions with CMAS–1 and CMAS–2 are listed in Table I. Figure 2(a) compares the expansion behavior for γ-YDS between scans of interactions with CMAS–1 and CMAS–2. The resulting $\Delta L/L_0$ plots lie on top of each other for the a and b directions. In the case of the c direction, the rate of change (slope) of the two experiments was effectively identical, but the absolute values of $\Delta L/L_0$ for CMAS–2 were higher. The cause of the offset in the c direction is not currently known, but this may be due to instrument error or sample displacement during measurement. It is also possible this difference could be attributed to stress and strain in the material as interactions between YDS and CMAS produce reaction products, although the average expansion measured for each direction of γ-YDS for samples exposed to CMAS–1 and CMAS–2 were equivalent.

TABLE I.—CALCULATED LATTICE PARAMETERS OF γ-$Y_2Si_2O_7$ FROM YDS:CMAS[a] IN SITU X-RAY DIFFRACTION SCANS

Sample	Temperature, °C	a, Å	b, Å	c, Å	γ	Volume, Å^3
YDS:CMAS–1[b]	25 (before)	5.5814	10.8392	4.6880	96.0322	282.0462
	500	5.5916	10.8643	4.6881	96.0440	283.2159
	900	5.6044	10.8921	4.6896	96.0783	284.6711
	1,100	5.6112	10.9091	4.6904	96.0923	285.4937
YDS:CMAS–2[c]	25 (before)	5.5814	10.8392	4.6880	96.0322	282.0462
	25 (after)	5.5812	10.8382	4.6800	96.0331	281.5341
	500	5.5916	10.8643	4.6881	96.0440	283.2159
	900	5.6044	10.8925	4.6896	96.0783	284.6711
	1,100	5.6112	10.9091	4.6904	96.0923	285.4937
	1,200	5.6149	10.9147	4.6916	96.1247	285.8896
	1,400	5.6207	10.9262	4.6933	96.1624	286.5717

[a]Yttrium disilicate:calcium-magnesium-aluminosilicate.
[b]CMAS–1 is 30.67CaO-8.25MgO-12.81$AlO_{1.5}$-48.27SiO_2.
[c]CMAS–2 is 24.82CaO-9.08MgO-14.24$AlO_{1.5}$-51.86SiO_2.

YbDS crystallizes in the β-$RE_2Si_2O_7$ structure, which is a monoclinic polymorph of the RE disilicates of space group *C2/m* and does not exhibit phase changes as a function of temperature. Lattice parameters of β-$Yb_2Si_2O_7$ are listed in Table II, and $\Delta L/L_0$ values for each lattice direction are plotted in Figure 2(b). The a direction of YbDS exhibited the greatest expansion and the c direction exhibited the lowest expansion. There was slight curvature of the expansion of the c direction near 1,400 °C, although overall, the expansion behavior in each direction appears to follow a linear trend. As shown in Table III, the calculated CTE values for YbDS were indicative of anisotropic expansion of this material at high temperatures and the average CTE was determined to be 4.82×10^{-6}/K.

TABLE II.—CALCULATED LATTICE PARAMETERS OF $Yb_2Si_2O_7$ FROM YbDS:CMAS–1[a] IN SITU X-RAY DIFFRACTION SCANS

Temperature, °C	a, Å	b, Å	c, Å	β	Volume, Å^3
25 (before)	6.7965	8.8730	4.7085	102.0052	277.7360
25 (after)	6.7992	8.8730	4.7077	101.9743	277.8331
500	6.8067	8.8828	4.7141	101.9671	278.8300
900	6.8240	8.8985	4.7199	101.9627	280.3857
1,100	6.8339	8.9098	4.7227	101.9703	281.3083
1,200	6.8387	8.9118	4.7240	101.9979	281.6186
1,400	6.8489	8.9208	4.7255	102.0266	282.3813

[a]Ytterbium disilicate:calcium-magnesium-aluminosilicate. CMAS–1 is 30.67CaO-8.25MgO-12.81$AlO_{1.5}$-48.27SiO_2.

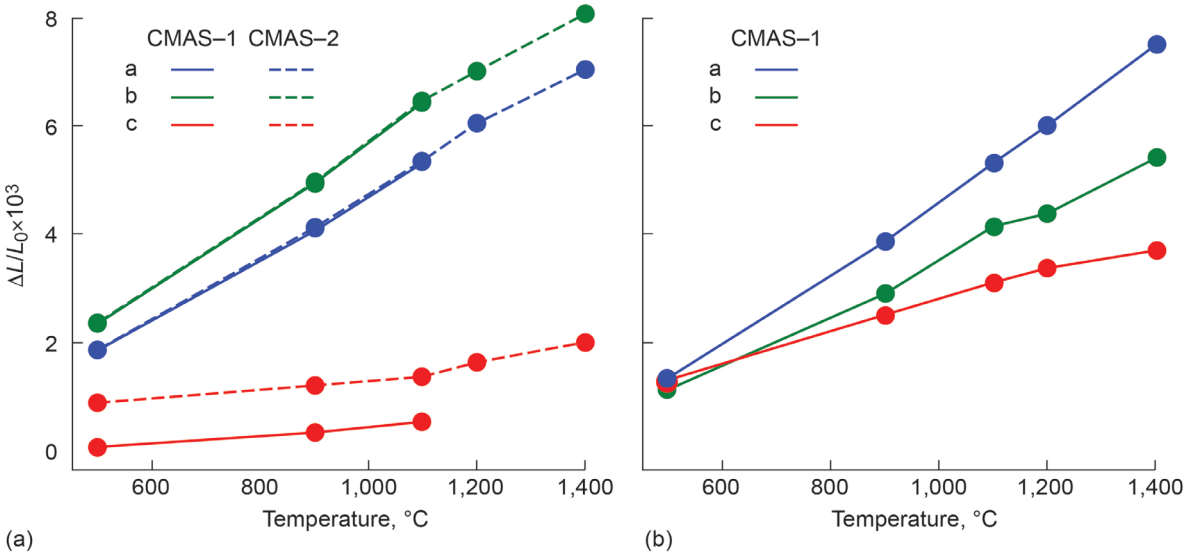

Figure 2.—Change in lattice parameter $\Delta L/L_0$ versus temperature plots for yttrium (YDS) and ytterbium (YbDS) disilicates. (a) γ-YDS. Calcium-magnesium-aluminosilicate (CMAS). CMAS–1 is 30.67CaO-8.25MgO-12.81$AlO_{1.5}$-48.27SiO_2. CMAS–2 is 24.82CaO-9.08MgO-14.24$AlO_{1.5}$-51.86SiO_2. (b) YbDS.

TABLE III.—AVERAGE THERMAL EXPANSION COEFFICIENT VALUES FROM 25 TO 1,400 °C FOR β-$YB_2SI_2O_7$ AND Γ-$Y_2SI_2O_7$ AND VALUES FROM LITERATURE

Material	α_a ($\times10^{-6}$)	α_b ($\times10^{-6}$)	α_c ($\times10^{-6}$)	Average	Literature
γ-$Y_2Si_2O_7$ (CMAS–1)[a]	5.84	6.80	0.81	4.49	~3.9 to 4.6 up to 1,200 °C[b]
γ-$Y_2Si_2O_7$ (CMAS–2)[c]	5.85	6.82	.81	4.49	
β-$Yb_2Si_2O_7$	6.89	4.81	2.78	4.82	~3.6 to 4.2 up to 1,600 °C[d]

[a]Calcium-magnesium-aluminosilicate (CMAS). CMAS–1 is 30.67CaO-8.25MgO-12.81$AlO_{1.5}$-48.27SiO_2.
[b]References 13 and 14.
[c]CMAS–2 is 24.82CaO-9.08MgO-14.24$AlO_{1.5}$-51.86SiO_2.
[d]Reference 15.

Literature values of average CTEs of YDS and YbDS are also listed in Table III, showing good agreement with the values measured in this investigation, although interestingly, the average CTE of YbDS is slightly higher than the values from previous studies. Like γ-YDS, possible instrument error or the presence of other phases in the sample and the resulting stress and strain states may be affecting the expansion behavior. However, the close comparison of these CTE values to data from literature substantiated the further use of these experiments to determine the CTEs of the Ca-RE apatites.

2.2 $Ca_2Y_8(SiO_4)_6O_2$ and $Ca_2Yb_8(SiO_4)_6O_2$

$Ca_2RE_8(SiO_4)_6O_2$ materials crystallize in the hexagonal space group $P6_3/m$, and the lattice parameters of $Ca_2Y_8(SiO_4)_6O_2$ are listed in Table IV. The average CTEs of the apatite materials (shown in Figure 3) assessed here are almost double of that observed for γ-YDS and β-YbDS over the investigated temperature range. The $\Delta L/L_0$ plots for the crystal directions that were calculated for $Ca_2Y_8(SiO_4)_6O_2$ exhibit small differences in slope between CMAS–1 and CMAS–2 (Figure 3(a)), with the CTEs listed in Table VI.

TABLE IV.—LATTICE PARAMETERS OF $CA_2Y_8(SIO_4)_6O_2$ CALCULATED FROM YDS:CMAS[a] IN SITU X-RAY DIFFRACTION SCANS

Sample	Temperature, °C	a, Å	c, Å	Volume, Å^3
YDS:CMAS–1[b]	25 (after)	9.3483	6.7771	512.9058
	1,200	9.4496	6.8439	529.2410
	1,400	9.4768	6.8571	533.3282
YDS:CMAS–2[c]	25 (after)	9.3436	6.7786	512.5137
	1,200	9.4442	6.8405	528.3903
	1,400	9.4654	6.8500	531.4991

[a]Yttrium disilicate:calcium-magnesium-aluminosilicate.
[b]CMAS–1 is 30.67CaO-8.25MgO-12.81$AlO_{1.5}$-48.27SiO_2.
[c]CMAS–2 is 24.82CaO-9.08MgO-14.24$AlO_{1.5}$-51.86SiO_2.

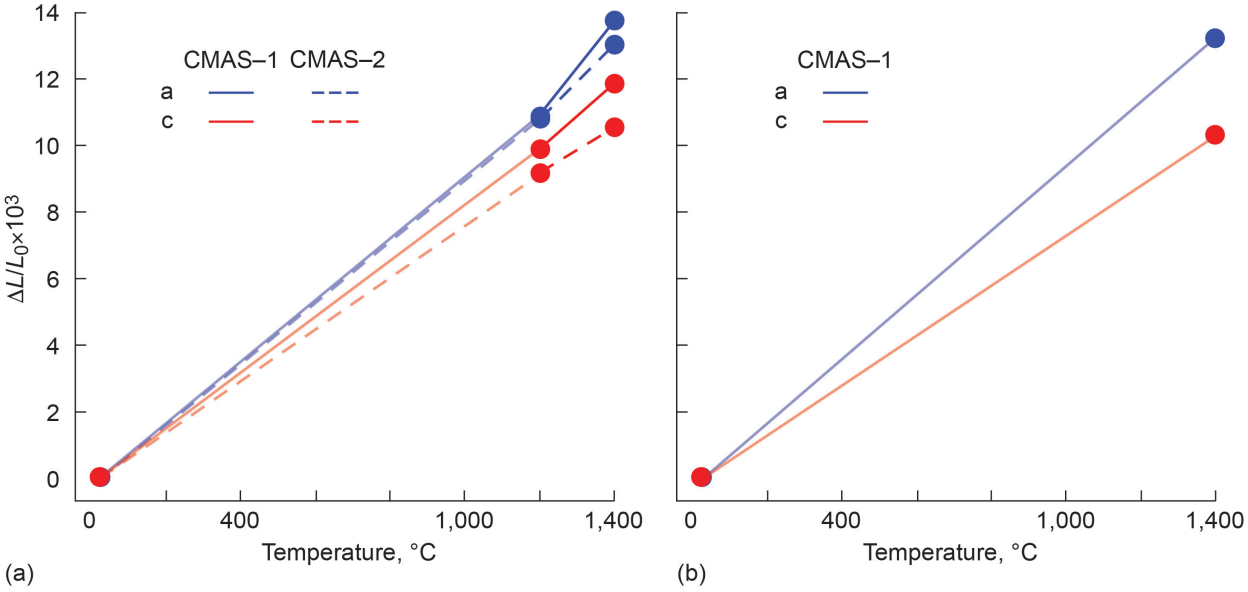

Figure 3.—Change in lattice parameter $\Delta L/L_0$ versus temperature plots for (a) $Ca_2Y_8(SiO_4)_6O_2$ and (b) $Ca_2Yb_8(SiO_4)_6O_2$. Faded lines in figure represent lack of data due to limited or no apatite crystallization between 25 and 1,200 °C in (a) and 25 and 1,400 °C in (b). Calcium-magnesium-aluminosilicate (CMAS). CMAS–1 is 30.67CaO-8.25MgO-12.81$AlO_{1.5}$-48.27SiO_2. CMAS–2 is 24.82CaO-9.08MgO-14.24$AlO_{1.5}$-51.86SiO_2.

TABLE V.—LATTICE PARAMETERS OF $Ca_2Yb_8(SiO_4)_6O_2$ CALCULATED FROM YbDS:CMAS–1[a] IN SITU X-RAY DIFFRACTION SCANS

Temperature, °C	a, Å	c, Å	Volume, Å^3
25 (after)	9.2935	6.7009	501.2212
1,400	9.4166	6.7696	519.8611

[a]Ytterbium disilicate:calcium-magnesium-aluminosilicate. CMAS–1 is 30.67CaO-8.25MgO-12.81$AlO_{1.5}$-48.27SiO_2.

TABLE VI.—AVERAGE LINEAR THERMAL EXPANSION COEFFICIENT VALUES FROM 25 TO 1,400 °C FOR $Ca_2Y_8(SiO_4)_6O_2$ AND $Ca_2Yb_8(SiO_4)_6O_2$

Material	α_a ($\times10^{-6}$)	α_c ($\times10^{-6}$)	Average
$Ca_2Y_8(SiO_4)_6O_2$ (CMAS–1)[a]	9.54	8.36	8.95
$Ca_2Y_8(SiO_4)_6O_2$ (CMAS–2)[b]	9.19	7.55	8.37
$Ca_2Yb_8(SiO_4)_6O_2$	9.63	7.45	8.54

[a]Calcium-magnesium-aluminosilicate (CMAS). CMAS–1 is 30.67CaO-8.25MgO-12.81$AlO_{1.5}$-48.27SiO_2.

[b]CMAS–2 is 24.82CaO-9.08MgO-14.24$AlO_{1.5}$-51.86SiO_2.

Only one data point was obtained for $Ca_2Yb_8(SiO_4)_6O_2$, as apatite was only formed in YbDS:CMAS–1 at 1,400 °C (Table V). Using these two data points and assuming linear expansion behavior, the calculated CTEs of the apatites are listed in Table VI.

3.0 Discussion

High-temperature x-ray studies provided the capability to measure the CTE of the EBC compositions as well as the $Ca_2Y_8(SiO_4)_6O_2$ and $Ca_2Yb_8(SiO_4)_6O_2$ reaction products. Close comparison to literature CTE values for the disilicates validated the use of these scans for the investigation of the expansion behavior of $Ca_2Y_8(SiO_4)_6O_2$ and $Ca_2Yb_8(SiO_4)_6O_2$. Although the thermal expansion of these particular Ca-RE apatites has not been previously investigated in literature, the results can be compared to the limited data on other apatite stoichiometries, which all crystallize in the hexagonal $P6_3/m$ structure. Misture et al. investigated the thermal expansion behavior of $Dy_{9.33}(SiO_4)_6O_2$, absent of Ca in the structure (Ref. 16). The average a and c CTEs in that study were determined to be 9.93×10^{-6}/K and 8.30×10^{-6}/K, respectively, up to 1,450 °C. Similarly, in a study by Key et al., the average CTEs of $Y_{9.33}(SiO_4)_6O_2$ were calculated as $\alpha_a = 8.98\times10^{-6}$/K and $\alpha_a = 8.45\times10^{-6}$/K up to 1,200 °C (Ref. 17). In both studies, the thermal expansion behavior was observed to be linear at ≥1,200 °C. This linear thermal expansion behavior is consistent with the Ca-containing apatite stoichiometries studied in this work, although data at additional temperatures are needed to confirm a linear expansion trend. Based on these literature values, there is not a large difference overall in CTE behavior of the Ca-RE apatites measured here compared to the RE apatites absent of CaO, although it will be crucial to perform these experiments on phase pure Ca-RE samples to corroborate the current findings, as the presence of other crystalline and amorphous phases might be skewing the data at a magnitude that cannot be accounted for at the current time. Overall, these limited results suggest that the Ca-RE apatites possess CTEs much higher than desired for EBC applications and this mismatch would be expected to generate undesirable stress states. The average thermal expansion behavior of these apatite systems is much closer to CTEs of TBCs (~10 to 14×10^{-6}/K) (Ref. 18). The anisotropy of the thermal expansion of these apatite materials is also not desirable for EBCs or TBCs, as the different rates of expansion can also result in microstrain and cracking.

4.0 Conclusions

The thermal expansion coefficients (CTEs) of $Ca_2Y_8(SiO_4)_6O_2$ and $Ca_2Yb_8(SiO_4)_6O_2$ were determined using in situ x-ray diffraction scans of thermochemical interactions of $Y_2Si_2O_7$ and $Yb_2Si_2O_7$ with two different calcium-magnesium-aluminosilicate (CMAS) compositions. CTEs were obtained for $Y_2Si_2O_7$ and $Yb_2Si_2O_7$ and compared favorably to literature values. The average bulk CTEs of $Ca_2Y_8(SiO_4)_6O_2$ and $Ca_2Yb_8(SiO_4)_6O_2$ were determined to be almost two times greater in magnitude than what is desirable for environmental barrier coating applications, but these materials have CTEs similar to thermal barrier coating materials. Additional in situ measurements of the calcium rare-earth (RE) apatites are needed to fully understand the expansion behavior at high temperature. The current measurements described herein correlate well with results of thermal expansion of other RE apatites in literature, which suggests that this method of measuring thermal expansion properties in situ with CMAS reactions can provide fairly accurate thermal property data.

References

1. Opila, Elizabeth J., et al.: SiC Recession Caused by SiO_2 Scale Volatility Under Combustion Conditions: II, Thermodynamics and Gaseous-Diffusion Model. J. Am. Ceram. Soc., vol. 82, no. 7, 1999, pp. 1826–1834.
2. Smialek, James L., et al.: SiC and Si_3N_4 Recession Due to SiO_2 Scale Volatility Under Combustor Conditions. Adv. Compos. Mater., vol. 8, no. 1, 1999, pp. 33–45.
3. Lee, K.N.; Fox, D.S.; and Bansal, N.P.: Rare Earth Silicate Environmental Barrier Coatings for SiC/SiC Composites and Si_3N_4 Ceramics. J. Eur. Ceram. Soc., vol. 25, 2005, pp. 1705–1715.
4. Lee, Kang N.: Environmental Barrier Coatings for SiC_f/SiC. Ceramic Matrix Composites: Materials, Modeling and Technology, Narottam P. Bansal and Jacques Lamon, eds., John Wiley and Sons, Hoboken, NJ, 2014, pp. 430–451.
5. Smialek, James L.: The Chemistry of Saudi Arabian Sand: A Deposition Problem on Helicopter Turbine Airfoils. NASA TM–105234, 1991. https://ntrs.nasa.gov
6. Borom, M.P.; Johnson, C.A.; and Peluso, L.A.: Role of Environmental Deposits and Operating Surface Temperature in Spallation of Air Plasma Sprayed Thermal Barrier Coatings. Surf. Coat. Tech., vol. 86–87, nos. 1–3, 1996, pp. 116–126.
7. Kim, J., et al.: Deposition of Volcanic Materials in the Hot Sections of Two Gas Turbine Engines. J. Eng. Gas Turbines Power, vol. 115, no. 3, 1993, pp. 641–651.
8. Stokes, Jamesa L., et al.: High-Temperature Thermochemical Interactions of Molten Silicates With $Yb_2Si_2O_7$ and $Y_2Si_2O_7$ Environmental Barrier Coating Materials. J. Eur. Ceram. Soc., vol. 39, no. 15, 2019, pp. 5059–5067.
9. Stokes, Jamesa L., et al.: Effects of Crystal Structure and Cation Size on Molten Silicate Reactivity With Environmental Barrier Coating Materials. J. Am. Ceram. Soc., vol. 103, no. 1, 2020, pp. 622–634.
10. Krämer, Stephan; Yang, James; and Levi, Carlos G.: Infiltration-Inhibiting Reaction of Gadolinium Zirconate Thermal Barrier Coatings With CMAS Melts. J. Am. Ceram. Soc., vol. 91, no. 2, 2008, pp. 576–583.
11. Coelho, Alan A.: TOPAS and TOPAS-Academic: An Optimization Program Integrating Computer Algebra and Crystallographic Objects Written in C++. J. Appl. Crystallogr., vol. 51, 2018, pp. 210–218.
12. Felsche, J.: Crystal Data on the Polymorphic Disilicate $Y_2Si_2O_7$. Naturwissenschaften, vol. 57, 1970, pp. 127–128.

13. Sun, Ziqi, et al.: Thermal Properties and Thermal Shock Resistance of γ-$Y_2Si_2O_7$. J. Am. Ceram. Soc., vol. 91, no. 8, 2008, pp. 2623–2629.
14. Dolan, M.D., et al.: Structures and Anisotropic Thermal Expansion of the α, β, γ, and δ Polymorphs of $Y_2Si_2O_7$. Powder Diffr., vol. 23, no. 1, 2008, pp. 20–25.
15. Fernández-Carrión, Alberto J.; Allix, Mathieu; and Becerro, Ana I.: Thermal Expansion of Rare-Earth Pyrosilicates. J. Am. Ceram. Soc., vol. 96, no. 7, 2013, pp. 2298–2305.
16. Misture, S.T., et al.: Synthesis, Crystal Structure, and Anisotropic Thermal Expansion of $Dy_{4.67}(SiO_4)_3O$. J. Mater. Res., vol. 19, no. 8, 2004, pp. 2330–2335.
17. Key, Thomas S., et al.: Total Thermal Expansion Coefficients of the Yttrium Silicate Apatite Phase $Y_{4.69}(SiO_4)_3O$. J. Am. Ceram. Soc., vol. 97, no. 1, 2014, pp. 28–31.
18. Padture, Nitin P.; Gell, Maurice; and Jordan, Eric H.: Thermal Barrier Coatings for Gas-Turbine Engine Applications. Science, vol. 296, no. 5566, 2002, pp. 280–284.